A novel hollowed CoO-in-CoSnO 3 nanostructure with enhanced lithium storage capabilities

Guan, Cao; Li, Xianglin; Yu, Hong; Mao, Lu; Wong, Lydia Helena; Yan, Qingyu; Wang, John

2014

https://hdl.handle.net/10356/81341

https://doi.org/10.1039/C4NR04505J

ARTICLE

A Novel Hollowed CoO-in-CoSnO₃ Nanostructure with Enhanced Lithium Storage Capabilities

Cao Guan*[a], Xianglin Li[b], Hong Yu[c], Lu Mao[a], Lydia Helena Wong[c], Qingyu Yan[c], and John Wang*[a]

Searching for well-defined porous/hollowed metal oxide nanocomposites is promising for high performance energy storage. Herein, atomic layer deposition (ALD) has been utilized for the construction of a novel hollowed wire-in-tube nanostructure of CoO-in-CoSnO₃, for which, $Co_2(OH)_2CO_3$ nanowires are firstly obtained by hydrothermal method and then deposited with ALD SnO_2. After a proper thermal treatment, a CoO wire-void-CoSnO₃ tube was formed with the decomposition of $Co_2(OH)_2CO_3$ and its simultaneous reaction with the outer SnO_2 layer. In this unique wire-in-tube structure, both CoO and $CoSnO_3$ are promising materials for lithium ion battery anodes with high theoretical capacities, and the *porous+hollow* feature is essential for better electrode/electrolyte contact, shorter ion diffusion path and better structure stability. After a further facile carbon coating, the hollowed wire-in-tube structure delivered an improved capacity of 1162.1 mAh/g, which is much larger than that of the bare CoO nanowire. Enhanced rate capability and cycling stability have also been demonstrated with the structure, showing its promising application for the anode material of lithium ion battery. The work also demonstrated an effective way of using ALD SnO_2 for electrochemical energy storage that it plays a key role in the structure formation and also serves as both active material and surface coating.

Introduction

Energy crisis and climate change in recent decades have brought about huge research concern on sustainable energy production and storage[1]. Lithium ion batteries (LIBs) are currently the most widely used energy storage devices since their superior properties such as high energy density, long cycle life and environment benignity[2]. Yet custom demands for high energy density and long cycling life LIBs in electric vehicles (EVs) or portable electronics is constantly driving research efforts for novel electrode materials with better electrochemical performance, such as high energy/power density, better rate capability, cycling stability, and safety[3,4]. Among the numerous materials studied for anodes, metal oxides have long been considered as promising substitute for currently utilized graphite because they can provide much higher capacity[5,6]. However, their drawbacks such as low electric conductivity and fast capacity fading prevent them from widely commercialization at present stage, thus rational and careful endeavors should be carried out to solve these problems.

To achieve high performance metal oxides anodes, not only proper materials should be carefully chosen, but also the accordingly structure of the material should be rationally designed to fully utilize the merits of the material and balance its shortcomings[5,7]. Recent years have witness worldwide research works on nanostructured metal oxides, especially with porous and hollow features, because they can offer better electrode/electrolyte contact, short ion diffusion length and reduce the mechanical stress, thus result in much improved electrochemical properties[8,9]. At the same time, novel nanostructures with different functional components(such as core-shell, stem-branch, yolk-shell, and segmented wires) with different methods have been developed for better performance materials and much improved properties have been reported with synergetic effects aroused from different components[7,10].

Among various nanotechnologies, atomic layer deposition (ALD) has drawn wide research concern for LIBs since its uniform and conformal coating with well controllable atomic-scale thickness, and many metal oxides by ALD have been successfully utilized and demonstrated their powerful usage for better LIBs[11-13]. One main direction of using ALD for LIBs is to take advantage of ALD for conformal surface protective coating on electrodes, which can stabilize the solid electrolyte interface (SEI) and enable better cycling ability[14-18]. Another strategy is depositing active materials by ALD on some 3D complex conductive substrates to obtain better performance, because the controllable thickness of active material with the conductive supporting can short ion diffusion length and ensure better electric conductivity[19-21]. Despite these efforts, an ALD induced well-defined metal oxide nanostructure with satisfactory cycling ability and high capacity is still highly desirable for next-generation LIBs.

Herein, we report a novel wire-in-tube structure of CoO-in-CoSnO₃ (CoO@CoSnO₃) obtained by ALD SnO_2 on $Co_2(OH)_2CO_3$ nanowire with the following thermal treatment. During the thermal annealing, part of the CoO reacted with the

outer SnO_2 layer forming a tube shell, and a voids gap was formed between the tube and the rest CoO core. In this way, a unique $CoO\Theta CoSnO_3$ structure which is constructed with porous CoO nanowire core, porous $CoSnO_3$ shell and a gap between them can be achieved. In this wire-in-tube structure, both CoO and $CoSnO_3$ are promising materials for lithium anodes with high theoretical capacities, and the *porous+hollow* feature of the structure is beneficial for better contact with electrolyte with shorter ion diffusion path, making this wire-in-tube structure promising for LIBs application. By applying a further facile carbon coating, the $CoO\Theta CoSnO_3@C$ can deliver a stable capacity of 695.7 mAh/g after 100 cycles, and the structure also show very good rate capability compared with bare CoO or CoO-SnO_2 core-shell nanostructure. The work also designed a novel hollowed nanostructure with the help of ALD, and ALD SnO_2 has been successfully utilized as both active material and surface coating for electrochemical energy storage.

Experimental

Material synthesis

(1) $Co_2(CO_3)(OH)_2$ nanowire was firstly synthesized on nickel foam by a hydrothermal process. In detail, 2 mmol $Co(NO_3)_2 \cdot 6H_2O$, 10 mmol urea and 2 mmol NH_4F were firstly dissolved in 50 mL deionized water under stirring until a homogeneous solution was obtained, then it was transferred into Teflon-lined stainless steel autoclave, in which a piece of clean nickel foam (20 * 50 * 0.1 mm^3, with upperside protected by uniformly polytetrafluoroethylene coating tape) was immersed. Then the reaction was carried out at 110 ºC for 6 h for the growth. (2) ALD coating of SnO_2 on the nickel foam with $Co_2(CO_3)(OH)_2$ nanowire was conducted on a Fiji 200 system using tetrakis(dimethylamino) tin (TDMASn or $Sn(N(CH_3)_2)_4$) and H_2O as precursors at 120 °C, with the TDMASn source kept at 60 °C to reach a proper vapor pressure during the deposition. The precursors were pulsed in the reactor with 40 SCCM (cubic centimeter per minute) constant Ar flow, and the base pressure for deposition was 0.8 torr. The pulse time for TDMASn and H_2O were 2 and 0.1 seconds, respectively, and the purge time for both precursors were 10 seconds. The ALD SnO_2 thin film thickness on flat Si substrate was measured using a SE (α-SE, J. A. Woollam). With 200 ALD SnO_2 cycles, the result thin film thickness is about 40 nm, which presents a growth rate per cycle of ~0.2 nm. Thus we deposit 50 cycles to obtain ~10 nm. (3) To obtain $CoO\Theta CoSnO_3$ wire-in-tube structure, the $Co_2(CO_3)(OH)_2@SnO_2$ was annealed in Ar at 450 ˚C for 2 h. (4) For the carbon coating, the material was immersed into 0.04 M glucose for 24 h then annealed in Ar at 450 °C for 2 h.

Material Characterization

All the samples were characterized by scanning electron microscopy (SEM, JSM-6700F, 5.0-10.0 kV), transmission electron microscopy (TEM, JEM-2010FEF, 200 kV), and X-ray photoelectron spectroscopy (XPS, PHI 5700). The mass of electrode materials was measured on an AX/MX/UMX Balance (METTLER TOLEDO, maximum=5.1 g; delta = 0.001 mg).

Electrochemical test

Electrochemical measurements were performed using two-electrode CR2032 (3 V) coin-type cells with lithium foil serving as both counter and reference electrodes under ambient temperature. The electrolyte was 1 M LiPF6 in a 50: 50 (w/w) mixture of ethylene carbonate (EC) and dimethyl carbonate (DMC). Cell assembly was carried out in an argon-filled glovebox with both moisture and oxygen contents below 1.0 ppm. Electrochemical tests were performed using a NEWARE battery tester at a voltage window of 0.005–2.5 V. Cyclic voltammetry (CV, 0.005–2.5 V, 0.5 mV s^{-1}) was performed using an electrochemical workstation (CHI 760D). Electrochemical Impedance Spectroscopy (EIS) is carried out at open circuit potential from 0.1-10 000Hz. The active material loading is ~3.7 mg/cm^2 for $CoO\Theta CoSnO_3@C$, ~3.5 mg/cm^2 for $CoO\Theta CoSnO_3$, and ~3 mg/cm^2 for bare CoO.

Results and Discussion

Fabrication and Characterization
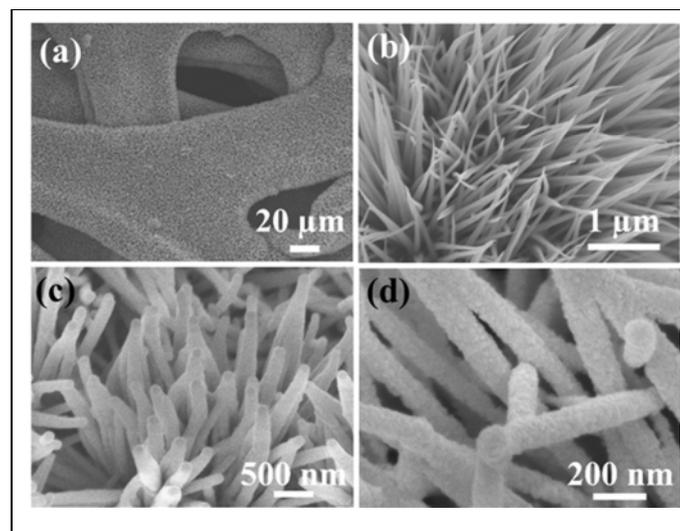
Fig. 1. SEM images of (a-b) $Co_2(OH)_2CO_3$ nanowire, (c) $Co_2(OH)_2CO_3@SnO_2$ obtained by ALD SnO_2 on $Co_2(OH)_2CO_3$, and (d) $Co_2(OH)_2CO_3@SnO_2$ after thermal treatment at 450 ^{0}C.

To achieve the wire-in-tube nanostructure, the precursor of CoO nanowire is firstly synthesized with hydrothermal method on nickel foam according to previous works[22]. As illustrated from SEM image in **Fig. 1**a, the $Co_2(CO_3)(OH)_2$ nanowires are uniformly distributed after the hydrothermal growth, which is in accordance with previous reports[23-25]. Enlarged picture of the $Co_2(CO_3)(OH)_2$ is shown in Fig. 1b, from which one can see the wires are smooth on the surface. After ALD coating of 10 nm SnO_2 on the surface, the nanowires become obvious larger, as shown in Fig. 1c, indicating $Co_2(CO_3)(OH)_2@SnO_2$ core-shell nanowires are obtained. The $Co_2(CO_3)(OH)_2@SnO_2$ nanowires are further thermal treated in argon at 450 °C, after which the wire-shaped structure is fully maintained, while its surface becomes quite rough and porous, as shown in Fig. 1d.

TEM experiment is carried out to provide more information on these structures. **Fig. 2**a shows the TEM image of a $Co_2(CO_3)(OH)_2@SnO_2$ core-shell nanowire, where the $Co_2(CO_3)(OH)_2$ is uniformly covered with a thin layer of SnO_2, indicating the conformal coating of ALD. After thermal treatment at 450 ˚C, as shown in Fig. 2b, the $Co_2(CO_3)(OH)_2@SnO_2$ becomes quite different and a wire-in-tube structure is formed. Since the thermal annealing of $Co_2(CO_3)(OH)_2$ alone will only result in porous CoO nanowires, and the tube thickness of the final wire-in-tube structure is much larger than 10 nm (which is the thickness of

SnO_2), we propose the SnO_2 reacts with the $Co_2(CO_3)(OH)_2$ during the thermal treatment. This reaction has been confirmed
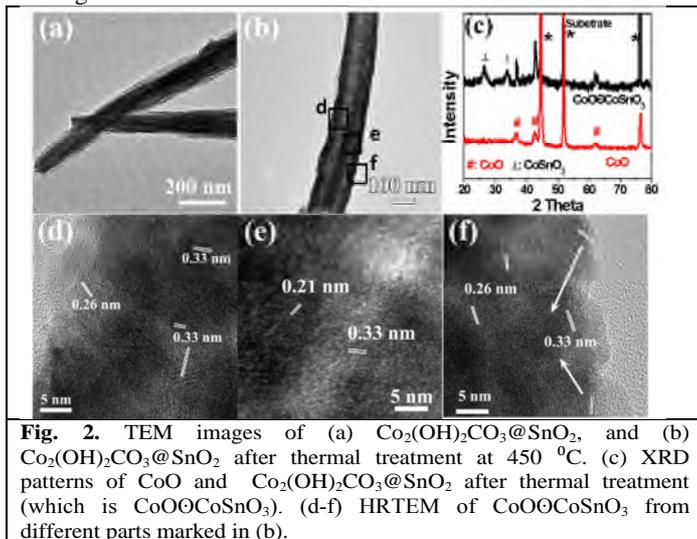

Fig. 2. TEM images of (a) $Co_2(OH)_2CO_3@SnO_2$, and (b) $Co_2(OH)_2CO_3@SnO_2$ after thermal treatment at 450 ^{0}C. (c) XRD patterns of CoO and $Co_2(OH)_2CO_3@SnO_2$ after thermal treatment (which is $CoO\ominus CoSnO_3$). (d-f) HRTEM of $CoO\ominus CoSnO_3$ from different parts marked in (b).

by XRD and HRTEM test, as shown in Fig. 2c-f. From XRD experiment results in Fig. 2c, we can see two peaks indicating $CoSnO_3$ but not SnO_2 appeared after the thermal treatment of $Co_2(CO_3)(OH)_2@SnO_2$, while only annealing of $Co_2(CO_3)(OH)_2$ resulted in CoO alone. Thus it can be seen from the XRD results that the wire-in-tube structure is formed by the decomposition of $Co_2(CO_3)(OH)_2$ to CoO and the simultaneously formation of $CoSnO_3$ shell. HRTEM is further carried out to confirm the results. From different parts marked in Fig. 2b, the shell lattice of 0.33 and 0.26 nm represents the $CoSnO_3$ (JCPDS, card no. 28-1236), and the core material shows a lattice fringe of 0.21 nm corresponding to CoO[26, 27], indicating the wire-in-tube structure is composed of CoO core and $CoSnO_3$ shell.
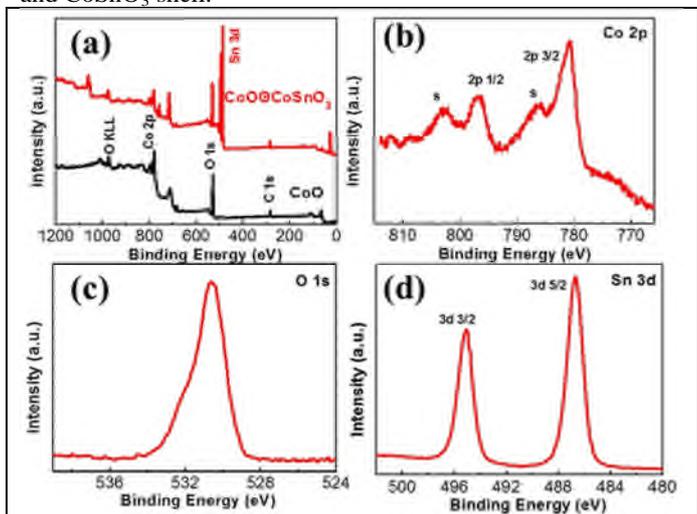

Fig. 3. XPS spectrum of (a) CoO and $CoO\ominus CoSnO_3$, and (b-d) Co 2p, O 1s and Sn 3d regions in $CoO\ominus CoSnO_3$.

To further characterize the component of the $CoO\ominus CoSnO_3$, XPS experiment is conducted and the result is shown in **Fig. 3**. From Fig. 3a, the $CoO\ominus CoSnO_3$ shows almost the same result as the CoO but with several additional peaks, which is due to the further deposition of SnO_2 with thermal treatment. Detailed scans of Co 2p, O 1s and Sn 3d range are illustrated in Figure 3b-d, respectively. From the Co 2p XPS spectrum in Fig. 3b, two peaks (Co 2p 3/2 and 2p 1/2) are located at 780.8 eV and

796.7 eV accompanied by a broad satellite peak, respectively. The result is in good agreement with previous report of Co^{2+}.[28, 29] And the principal peak of O 1s is approximately located at 530.4 eV, which can be well ascribed to the metal oxide form (O^{2-}).[29] For the Sn 3d spectrum, two peaks (Sn 3d 5/2, Sn 3d 3/2) are centering at 486.6 and 495.1 eV, respectively, which is in accordance with the electronic state of Sn^{4+}.[30] In both the XPS spectra of CoO and $CoO\ominus CoSnO_3$, no Co^{3+} or Sn^{2+} is observed.
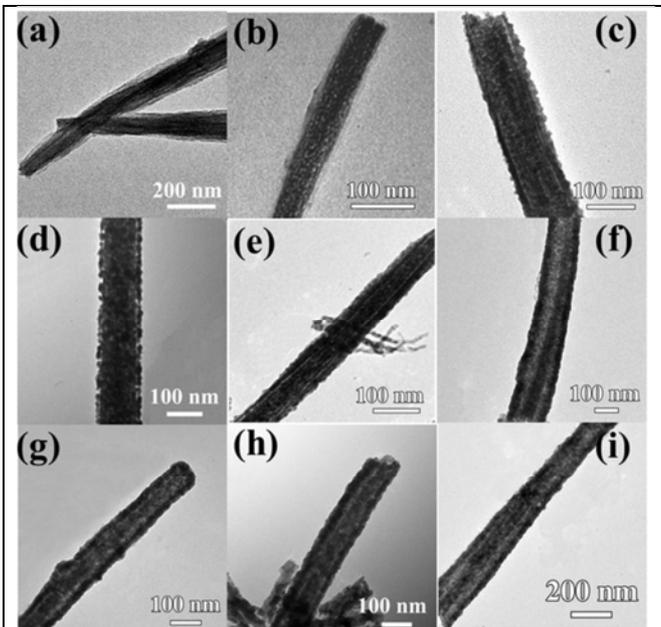

Fig. 4. TEM images of the $Co_2(OH)_2CO_3@SnO_2$ after thermal treatment at different temperatures of: (a) room temperature, (b) 250, (c) 300, (d) 350, (e) 400, (f) 450, (g) 550, (h) 650, and (i) 750^{0}C.

To further understand the formation of the wire-in-tube structure, controlled experiment is carried out by changing the annealing temperature of $Co_2(CO_3)(OH)_2@SnO_2$ and the results are illustrated in **Fig. 4 and SFig. 1**. We can find out that if the annealing temperature is below 250 °C, only the $Co_2(CO_3)(OH)_2$ begin to decompose and become porous. When the temperature increases to the range of 250-400 °C, the reaction of SnO_2 with the inside material starts, along with the shell becoming porous and thicker. If we further increase the temperature to 450 °C, the wire-in-tube structure will be formed and it remains unchanged even when the temperature goes up to 750 °C. Further heat treatment at higher temperature may result in fully hollowed tube structure with Kirkendall effect[31, 32], but at high temperature the substrate may be damaged and the LIB performance of CoO will

be very poor, thus here we just choose the wire-in-tube structure obtained at 450 °C for the following study.

Based on the above results, the generation of the wire-in-tube structure from the initial core-shell nanowires is accompanied with the decomposition of $Co_2(CO_3)(OH)_2$, and its reconfiguration with the shell SnO_2 during the annealing at proper temperature. During the annealing process, the CoO will diffuse outside by react with SnO_2 layer, which is faster than the diffusion inside of the SnO_2, thus generating of a hollowed wire-in-tube structure. This process has certain similar parts to previously reported hollowed nanostructures by solid state reaction and diffusion[31, 33]. But in the formation of the wire-in-tube structure, only part of inner material reacts with the shell while the rest part of the core is fully maintained. This result is

different from previously reported $CoO@CoTiO_3$ nanotube[33], where inside core fully moves outward generating a double-shelled tube, and it is also different from ZnO/Al_2O_3, where inside core becomes segmented when excessive inner material of ZnO is involved[31]. The hollowed wire-in-tube structure of CoO-in-$CoSnO_3$ is also different from previous work of hollowed $CoO\ominus TiO_2$ core-shell structure, which involves a sacrificial layer and the followed etching process[27].
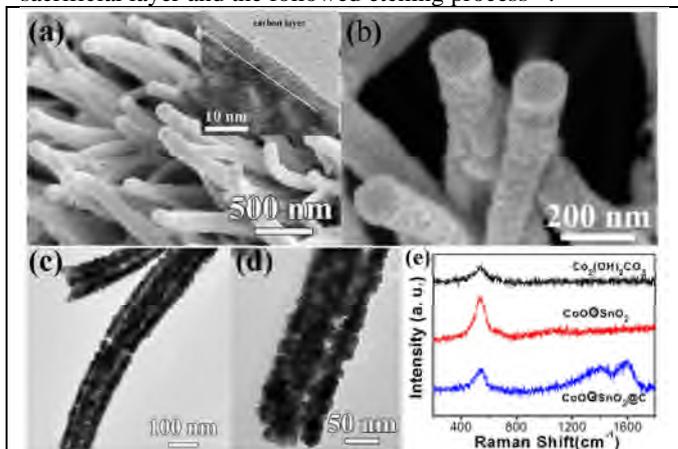

Fig. 5. (a-b) SEM and (c-d) TEM images of $CoO\ominus CoSnO_3$ after carbon coating. Inset in (a) showing HRTEM image of the carbon layer. (e) Raman spectrum of the three materials: $Co_2(OH)_2CO_3$, $CoO\ominus CoSnO_3$, and $CoO\ominus CoSnO_3$ with carbon coating.

In the wire-in-tube structure of $CoO\ominus CoSnO_3$, both the CoO and $CoSnO_3$ are promising anode materials for LIBs with high theoretical capacities, and the *porous+hollow* feature is beneficial for high electrolyte-electrode contact and the accommodation of severe strain generated during charge-discharge[34]. In the following step, we further carried out a facile carbon coating method that is usually utilized for metal oxide electrodes on this wire-in-tube structure, and investigate its lithium storage behavior.

The morphology of the structure after carbon coating is shown in **Fig. 5**a-b, from which we can see the wire-in-tube structure is well preserved while its surface becomes much rougher, which is consistent with previous reported result on carbon coated $CoSnO_3$ nanobox[35]. TEM experiment (Figure 5c-d) also shows the well-maintained wire-in-tube structure and a thin layer (less than 10 nm) of carbon is coated on the surface. The carbon coating is further investigated by Raman spectrum, as shown in Fig. 5e. After the carbon coating, the nanostructure shows two additional strong carbon-related peaks at ~1596 cm^{-1} (G band) and 1402 cm^{-1} (D band), demonstrating the sucessful amphrous carbon coating[35, 36]. XPS results in **Sfig. 2** also shows the carbon coating has not changed the states of Co 2p, O 1s and Sn 3d.

Lithium-ion battery test

In the following part, the electrochemical properties of the three materials: CoO, $CoO\ominus CoSnO_3$ and $CoO\ominus CoSnO_3@C$ have been investigated. **Fig. 6**a-c shows the differential capacity curves of the three materials. All the three curves have a significant peak at ~0.5 V which is mainly related to the formation of SEI during the first discharge, and a redox peaks at ~1.5/~2.2 V in the second cycle corresponding to the reaction of CoO with Li$^+$.[33] For the $CoO\ominus CoSnO_3$ and $CoO\ominus CoSnO_3@C$, an additional pair of peaks at ~1.0/~1.2 V

are associated with the reaction of Sn^{4+} with Li$^+$ during the process[37], showing the contribution from $CoSnO_3$, and the small intensity of the peaks indicate a low mass ratio of Sn^{4+} compared with Co^{2+}. Fig. 6d-f further shows the galvanostatic charge–discharge curves of the three materials at a current density of 400 mA/g. From the first cycle, the initial capacities of the CoO, $CoO\ominus CoSnO_3$ and $CoO\ominus CoSnO_3@C$ are 1085.5, 1234.9 and 1162.1 mAh/g, respectively. All of these capacities are much higher than the
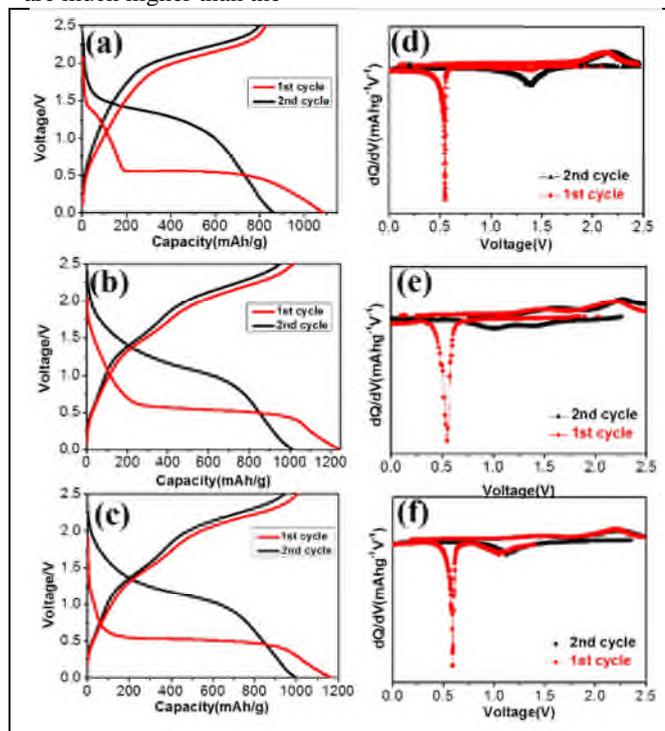

Fig. 6. (a-c) CV and (d-f) differential capacity curves of the three structures: CoO, $CoO\ominus CoSnO_3$, $CoO\ominus CoSnO_3@C$, respectively.
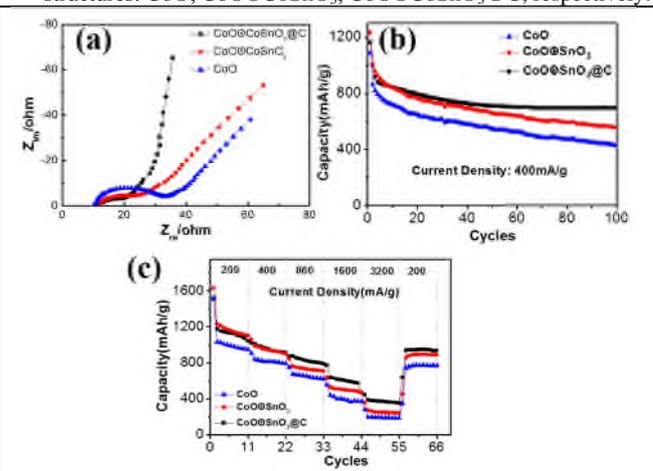
Fig. 7. (a) EIS, (b) cycling stability and (c) rate capability of the three structures: CoO, $CoO\ominus CoSnO_3$, $CoO\ominus CoSnO_3@C$, respectively.

theoretical value for CoO and $CoSnO_3$, and the ultrahigh capacity can be mainly due to the formation of SEI in the first discharge process, which have been reported on Co and Sn based oxides.[38-40] In the second cycle, the $CoO\ominus CoSnO_3$ delivers a capacity of 1004.7 mAh/g, which is much larger than

that of the bare CoO (861.2 mAh/g), and the value is also larger than previously reported $Co_3Sn_2@Co$ and Co_2SnO_4 nanoparticles[41] and a Sn-Co-CNT@CNT nanocomposite[42]. The improved capacity of the $CoO\Theta CoSnO_3$ can be attributed to its unique wire-in-tube structure, where the porous tube and core can enlarge the reaction area leading to better material utilization, and the hollow gap can allow easier penetration of the electrolyte. The capacity of $CoO\Theta CoSnO_3@C$ in the second cycle (996.4 mAh/g) is also much larger than that of CoO alone. The columbic efficiency of the CoO, $CoO\Theta CoSnO_3$ and $CoO\Theta CoSnO_3@C$ in the first cycle is 75.8%, 81.9%, and 86.7%, respectively. The low columbic efficiency can be from the irreversible reduction of metal oxide and the formation of SEI. We can still see the hollowed nanostructures shows better reaction reversibility, and carbon coating can further improve the columbic efficiency.

Electrochemical impendence spectroscopy (EIS) of the three structures are shown in **Fig. 7**a. Although all the three materials expressed similar bulk resistance (indicated by the intersection of the curve at real part), the $CoO\Theta CoSnO_3$ and $CoO\Theta CoSnO_3@C$ showed less charge-transfer resistance than bare CoO, as their diameters of the semi-cycle are less than that of the CoO. In addition, in the low frequency region, the slope of the $CoO\Theta CoSnO_3@C$ curve is closest to the imaginary axis, which demonstrated its lowest diffusion resistance. The improved conductivity for charge-transfer and ion diffusion can be originated from the porous/hollowed structure and the conductive carbon coating, which will be highly responsible for enhanced electrochemical properties.

The rate capability and cycling ability of the three materials are further tested and shown in Fig. 7b-c. At a current density of 400 mA/g, both $CoO\Theta CoSnO_3$ and $CoO\Theta CoSnO_3@C$ illustrate better capacity retention than that of bare CoO after 100 charge-discharge cycles. To verify the merits of hollowed, ALD SnO_2 was directly deposited on CoO nanowire to form a solid CoO-SnO_2 core-shell structure, yet it can only show a very limited cycling ability (**SFig. 3**). For $CoO\Theta CoSnO_3@C$, a capacity of 695.7 mAh/g can be still maintained after 100 cycles, corresponding to ~59.9 % of the first discharge capacity. While the CoO and $CoO\Theta CoSnO_3$ have a capacity retention of ~39.2% and 44.7 %, respectively. The improved cycling stability can be mainly related to the carbon coating, which can increase the electrode conductivity and alleviate the stress during the cycling[43]. Further improvement can be proposed if other carbonaceous materials can be utilized for the surface conductive coating, such as CNT and graohene[44-46].

The rate capability of $CoO\Theta CoSnO_3@C$ is also better than the bare CoO and $CoO\Theta CoSnO_3$, as shown in Fig. 7c. When the current density becomes higher all the three materials shows decreased capacity, owning to the limited reaction kinetics of metal oxides with electrolyte under high current[5]. When a high current density of 3200 mA/g is applied, the capacity of $CoO\Theta CoSnO_3@C$ is 388.9 mAh/g, which is higher than that of $CoO\Theta CoSnO_3$ (271.4 mAh/g) and bare CoO (195.7 mAh/g). And when the current density finally returns to 200 mA/g, the wire-in-tube structure shows the best capacity recover ability. The improved rate capability of the $CoO\Theta CoSnO_3@C$ can be attributed to (1) the hollowed structure with higher surface area for better electrode/electrolyte contact and faster electrochemical reaction under high current, and (2) the conductive carbon coating which can further improve the conductivity and reaction reversibility, and prevent the collapse of the structure, thus the $CoO\Theta CoSnO_3@C$ shows the best performance in electrochemical tests.

Conclusions

A novel *porous+hollowed* wire-in-tube structure is obtained by ALD SnO_2 on $Co_2(OH)_2CO_3$ nanowire with the following thermal annealing process. The solid-state reaction between SnO_2 and partially CoO will form a $CoSnO_3$ tube layer at proper temperature, leading to a novel CoO wire in $CoSnO_3$ tube structure. The unique *porous+hollow* feature of the $CoO\Theta CoSnO_3$ can short ion/charge diffusion length and facilitate electrode/electrolyte contact with more surface area, thus result in much better electrochemical performance compared with the bare CoO nanowire. After a facile carbon coating, the $CoO\Theta CoSnO_3@C$ demonstrates high capacity, very good cycling ability and rate capability, which is very promising for high performance lithium ion battery. The work also provides an effective way to utilize ALD for the construction of novel nanostructures and successfully demonstrates its promising application for electrochemical energy storage.

Notes and references

[a] Department of Materials Science and Engineering, National University of Singapore, 117574 Singapore.

[b] Energy Research Institute @ NTU, Nanyang Technological University, 50 Nanyang Drive, Research Techno Plaza, X-Frontier Block, Level 5, 637553 Singapore.

[c] School of Materials Science and Engineering, Nanyang Technological University, 639798 Singapore.

† Footnotes should appear here. These might include comments relevant to but not central to the matter under discussion, limited experimental and spectral data, and crystallographic data.

Electronic Supplementary Information (ESI) available: additional SEM images, XPS result and battery test result. See DOI: 10.1039/b000000x/

1. N.-S. Choi, Z. Chen, S. A. Freunberger, X. Ji, Y.-K. Sun, K. Amine, G. Yushin, L. F. Nazar, J. Cho and P. G. Bruce, *Angewandte Chemie International Edition*, 2012, 51, 9994-10024.

2. P. G. Bruce, B. Scrosati and J.-M. Tarascon, *Angewandte Chemie International Edition*, 2008, 47, 2930-2946.

3. G. Zhou, F. Li and H.-M. Cheng, *Energy & Environmental Science*, 2014, DOI: 10.1039/C3EE43182G.

4. R. Mukherjee, R. Krishnan, T.-M. Lu and N. Koratkar, *Nano Energy*, 2012, 1, 518-533.

5. J. Jiang, Y. Li, J. Liu, X. Huang, C. Yuan and X. W. Lou, *Advanced Materials*, 2012, 24, 5166-5180.

6. L. Ji, Z. Tan, T. Kuykendall, E. J. An, Y. Fu, V. Battaglia and Y. Zhang, *Energy & Environmental Science*, 2011, 4, 3611-3616.

7. C. Cheng and H. J. Fan, *Nano Today*, 2012, 7, 327-343.

8. C. Jiang, E. Hosono and H. Zhou, *Nano Today*, 2006, 1, 28-33.

9. C. Guan, X. Wang, Q. Zhang, Z. Fan, H. Zhang and H. J. Fan, *Nano Letters*, 2014, 14, 4852-4858.

10. W. Shi, X. Rui, J. Zhu and Q. Yan, *The Journal of Physical Chemistry C*, 2012, 116, 26685-26693.

11. X. Meng, X.-Q. Yang and X. Sun, *Advanced Materials*, 2012, 24, 3589-3615.

12. J. W. Elam, N. P. Dasgupta and F. B. Prinz, *MRS Bulletin*, 2011, 36, 899-906.

13. C. Marichy, M. Bechelany and N. Pinna, *Advanced Materials*, 2012, 24, 1017-1032.

14. D. Guan, J. A. Jeevarajan and Y. Wang, *Nanoscale*, 2011, 3, 1465-1469.

15. Y. S. Jung, A. S. Cavanagh, L. A. Riley, S.-H. Kang, A. C. Dillon, M. D. Groner, S. M. George and S.-H. Lee, *Advanced Materials*, 2010, 22, 2172-2176.

16. M. Liu, X. Li, H. Ming, J. Adkins, X. Zhao, L. Su, Q. Zhou and J. Zheng, *New Journal of Chemistry*, 2013, 37, 2096-2102.

17. H. Kim, J. T. Lee, D.-C. Lee, A. Magasinski, W.-i. Cho and G. Yushin, *Advanced Energy Materials*, 2013, 3, 1308-1315.

18. J.-H. Jeun, K.-Y. Park, D.-H. Kim, W.-S. Kim, H.-C. Kim, B.-S. Lee, H. Kim, W.-R. Yu, K. Kang and S.-H. Hong, *Nanoscale*, 2013, 5, 8480-8483.

19. J. M. Haag, G. Pattanaik and M. F. Durstock, *Advanced Materials*, 2013, 25, 3238-3243.

20. X. Li, X. Meng, J. Liu, D. Geng, Y. Zhang, M. N. Banis, Y. Li, J. Yang, R. Li, X. Sun, M. Cai and M. W. Verbrugge, *Advanced Functional Materials*, 2012, 22, 1647-1654.

21. S. Boukhalfa, K. Evanoff and G. Yushin, *Energy & Environmental Science*, 2012, 5, 6872-6879.

22. C. Guan, J. Liu, C. Cheng, H. Li, X. Li, W. Zhou, H. Zhang and H. J. Fan, *Energy & Environmental Science*, 2011, 4, 4496-4499.

23. X. Qing, S. Liu, K. Huang, K. Lv, Y. Yang, Z. Lu, D. Fang and X. Liang, *Electrochimica Acta*, 2011, 56, 4985-4991.

24. Y. Cui, Z. Wen and Y. Liu, *Energy & Environmental Science*, 2011, 4, 4727-4734.

25. C. Guan, Z. Zeng, X. Li, X. Cao, Y. Fan, X. Xia, G. Pan, H. Zhang and H. J. Fan, *Small*, 2014, 10, 300-307.

26. J. Jiang, J. Liu, R. Ding, X. Ji, Y. Hu, X. Li, A. Hu, F. Wu, Z. Zhu and X. Huang, *The Journal of Physical Chemistry C*, 2009, 114, 929-932.

27. C. Guan, X. Xia, N. Meng, Z. Zeng, X. Cao, C. Soci, H. Zhang and H. J. Fan, *Energy & Environmental Science*, 2012, 5, 9085-9090.

28. M. Hassel and H.-J. Freund, *Surface Science Spectra*, 1996, 4, 273-278.

29. M. W. Nydegger, G. Couderc and M. A. Langell, *Applied Surface Science*, 1999, 147, 58-66.

30. J. Huang, L. Wang, C. Gu, M. Zhai and J. Liu, *CrystEngComm*, 2013, 15, 7515-7521.

31. H. Jin fan, M. Knez, R. Scholz, K. Nielsch, E. Pippel, D. Hesse, M. Zacharias and U. Gosele, *Nat Mater*, 2006, 5, 627-631.

32. Y. Yin, R. M. Rioux, C. K. Erdonmez, S. Hughes, G. A. Somorjai and A. P. Alivisatos, *Science*, 2004, 304, 711-714.

33. J. Jiang, J. Luo, J. Zhu, X. Huang, J. Liu and T. Yu, *Nanoscale*, 2013, 5, 8105-8113.

34. C. Liu, F. Li, L.-P. Ma and H.-M. Cheng, *Advanced Materials*, 2010, 22, E28-E62.

35. Z. Wang, Z. Wang, W. Liu, W. Xiao and X. W. Lou, *Energy & Environmental Science*, 2013, 6, 87-91.

36. X. Lu, T. Liu, T. Zhai, G. Wang, M. Yu, S. Xie, Y. Ling, C. Liang, Y. Tong and Y. Li, *Advanced Energy Materials*, 2014, 4, n/a-n/a.

37. V. Aravindan, K. B. Jinesh, R. R. Prabhakar, V. S. Kale and S. Madhavi, *Nano Energy*, 2013, 2, 720-725.

38. Y. Wang, H. J. Zhang, L. Lu, L. P. Stubbs, C. C. Wong and J. Lin, *ACS Nano*, 2010, 4, 4753-4761.

39. Y. Li, B. Tan and Y. Wu, *Nano Letters*, 2007, 8, 265-270.

40. P. Wu, N. Du, H. Zhang, J. Yu and D. Yang, *The Journal of Physical Chemistry C*, 2010, 114, 22535-22538.

41. N. Mahmood, C. Zhang, F. Liu, J. Zhu and Y. Hou, *ACS Nano*, 2013, 7, 10307-10318.

42. Y. Gu, F. Wu and Y. Wang, *Advanced Functional Materials*, 2013, 23, 893-899.

43. Y. Qi, H. Zhang, N. Du, C. Zhai and D. Yang, *RSC Advances*, 2012, 2, 9511-9516.

44. F. D. Wu and Y. Wang, *Journal of Materials Chemistry*, 2011, 21, 6636-6641.

45. W. Sun and Y. Wang, *Nanoscale*, 2014, DOI: 10.1039/C4NR02999B.

46. W. Zhou, J. Zhu, C. Cheng, J. Liu, H. Yang, C. Cong, C. Guan, X. Jia, H. J. Fan, Q. Yan, C. M. Li and T. Yu, *Energy & Environmental Science*, 2011, 4, 4954-4961.